UNIVERSITY OF CALIFORNIA SAN DIEGO

Design and fabrication of locomotive robot driven by prismatic pouch actuators that generate multi-directional motion

A thesis submitted in partial satisfaction of the
requirements for the degree Master of Science

in

Engineering Sciences (Mechanical Engineering)

by

Jordan Banh

Committee in charge:

Professor Nicholas Gravish, Chair
Professor Shengqiang Cai
Professor Michael Tolley

2022

The Thesis of Jordan Banh is approved, and it is acceptable in quality and form for publication on microfilm and electronically.

University of California San Diego

2022

DEDICATION

I am dedicating this work to my parents and family who have supported and encouraged me throughout all my endeavors. They've helped me build a foundation that allows me to pursue my dreams and success.

EPIGRAPH

The most important thing is to try and inspire people so that they can be great in whatever they want to do.

Kobe Bryant

TABLE OF CONTENTS

LIST OF FIGURES

ACKNOWLEDGEMENTS

I would like to thank all the members of Gravish Lab for the encouragement and support throughout my time as a graduate student. It has been a pleasure to research and learn with all the members of Gravish Lab. I would like to especially thank my committee chair, Nicholas Gravish, for all his support and unwavering positivity.

Chapter 1, in part, uses material as it appears in Monolithic Fabrication of Printable Pouch Actuators Shuhang Zhang, Jordan Banh, Nick Gravish. The thesis author is the coauthor of this material.

This work was supported by the National Science Foundation under Grant No. (1935324).

VITA

2019 Bachelor of Science, University of California San Diego

2022 Master of Science, University of California San Diego

FIELDS OF STUDY

Major Field: Mechanical Engineering (Design)

ABSTRACT OF THE THESIS

Design and fabrication of locomotive robot driven by prismatic pouch actuators that generate multi-directional motion

by

Jordan Banh

Master of Science in Engineering Sciences (Mechanical Engineering)

University of California San Diego, 2022

Professor Nicholas Gravish, Chair

This paper describes the design and fabrication of a pneumatically powered locomotive robot that utilizes printable prismatic pouch motors to generate multi-directional motion of the legs. The pneumatic circuitry and pouch motor layout are integrated into the robot design and create a motion sequence that results in locomotion. The fabrication process of this robot consists of a combination of lamination, mask heat pressing, 3-d printing, and 2-dimensional plotting. The integrated pouch actuators of the robot can provide up to 5 N of block force using 25 kPa of air pressure supply. Optimal locomotion performance of the robot is found through experimentation with cycle frequency. The tethered robotic system is able to reliably carry

payloads up to 1250 grams. Untethered robot locomotion in the positive and negative x-direction was demonstrated. Finally, we demonstrated that the robot can be designed to walk laterally and longitudinally.

Chapter 1

Introduction

Robotics research has rapidly developed and technological advancements in robotics research have led to a myriad of robotic systems that are able to navigate extreme environments, confined spaces, and human-robot collaborative areas. Capabilities of robots have progressed in locomotion, object manipulation, and manufacturing [2]. The next advancement in robotic development that will increase the application of robots is the ability to navigate natural environments safely and adapt to various scenarios. The inherent compliance of soft robotics and soft components is well suited for scenarios that require safe interactions with the environment in unpredictable scenarios [5]. Soft robots are capable of utilizing simple methods of actuation to produce robust locomotive gaits [10]. Brown et al. have also designed a granular jamming gripper that is able to conform to various sizes and pick up unfamiliar objects [1]. Many researchers have also focused on the understanding of biological mechanisms to inspire solutions that are more efficient and robust. Karipoth et al. have researched a bioinspired worm-like robot with integrated strain sensing for sensory-feedback-based control. However, current robotic systems are generally unable to outperform their biological counterparts in terms of adaptability and extreme environment navigation[4].

Rapid prototyping is becoming an increasingly important aspect of robotic development. It allows for expedited testing and iterative design. Many robotic systems require complex fabrication processes and expensive materials. The design of cheaper, more accessible robot

fabrication processes will give a larger population the ability to create unique robotic systems and act a catalyst to innovation as well as education in robotics. The increased availability of 3D printers has proven to be a great tool to develop and train the next generation of engineers, scientist, and designers [11].

In this chapter, a variety of actuators designs and fabrication processes that are commonly used in robotic systems will be generally reviewed. Then previous work on the design and fabrication of pouch actuators are described. In the next chapter, prismatic pouch actuation is introduced and the performance is characterized. Then, this paper introduces a novel pouch actuated robot that is capable of locomotion with payloads that up to four times its chassis weight.

1.1 Various actuator designs and fabrication processes

1.1.1 Various actuator fabrication processes

Fused deposition modelling

3D printing methods provide tools to rapidly prototype complex structures and are more accessible than ever before. It has allowed for the customization of small batch quantities for relatively low costs. Fused deposition modelling (FDM) is one of the most common methods of additive manufacturing. The FDM method uses a thermoplastic polymer filament that is pushed through a heated nozzle to print layers of materials successively. The heated thermoplastic material fuses with the previous layer and solidifies once it has cooled down. FDM is relatively simple process that is cheap and quick. It is important to note that a significant downfall of FDM is that inter-layer distortion can cause mechanical weaknesses in the final product. [7]

Stereolithography

Stereolithogrpahy (SLA) uses UV light to convert monomers, which are in a solution or resin layer, to polymer chains. The pattern of polymers solidifies and holds successive layers. The material that is not polymerized is removed once the printing is completed. In order to

achieve greater mechanical performance, post-process thermal treatment or photo-curing is used. SLA is generally used to print very high-quality parts with fine details. Unfortunately ,it is a relatively slow process and expensive. [7]

Laminated object manufacturing

Laminated object manufacturing (LOM) uses layer-by-layer cutting and lamination of sheet materials. The layers are cut using tools such as mechanical cutters or lasers. Each successive layer is then bonded and formed. A variety of different material, such as metal, polymer composites, ceramics are used in LOM. LOM is great for building larger items and structures and is relatively quick. However, it has lower dimensional accuracy and can have time consuming post-processing steps for complex design shapes. [7]

Shape deposition manufacturing

Shape deposition manufacturing (SDM) is a fabrication process that builds up parts though alternating layers of structural and support material. It is a fabrication process that is used for both rigid and soft structures. It allows for the integration of different materials and embedded electronics by using a hybrid process that employs machining as well as molding. The machining allows for the fabrication of high precision details but is fairly time consuming and complex. [3][9] [12]

Soft lithography

Soft lithography is a low cost fabrication process for manufacturing structures on the micro- and nano-scale. Soft lithography fabricates these structures using an elastomeric stamp. Soft lithography is a great method for generating high throughput, but other lithography methods are needed to create the soft lithography stamp master. Fluidic Elastomeric actuators have been fabricated using the soft lithography method. [6]

1.1.2 Fluidic actuator designs

Pneumatic artificial muscles are a common actuator used for robotic applications. The most common Pneumatic Artificial Muscle (PAM) is the Mckibben type PAM which is made up of an elastic tube and braided sleeve. The tube is pressurized which leads to an expansion in the tube volume and diameter. The woven sleeve acts as a geometrical constraint which results in a contraction of the actuator length. These actuators can only exclusively generate a contraction or extension depending on the design and input pressure. Unfortunately, PAMs requires intricate manual fabrication processes.

Fluidic elastomer actuators use low durometer rubber that have embedded channels that are pressurized to generate a variety of motion primitives. The most common use for FEA is for bending. The basic structure for bending FEA is 2 elastic layers that are separated by a strain limiting layer. When either elastic side of the actuator is pressurized, it generates a bending motion due to the strain of the elastic layer and the constraint of the strain-limiting layer.[6]

1.2 Pouch motor design and fabrication

Pouch motors were initially introduced and researched by Niiyama et al. [8]. The basic fabrication process of the pouch motors is heat bonding two layers of sheet material with mechanical pressure. They design two different pouch fabrication processes that include fabrication by stamping and by drawing. The stamping process requires a machined printing block that is attached to the heating element of a heat press. This process is well suited for manufacturing large quantities for a design that is not expected to change because the machined block is not adjustable.

However, fabrication by drawing is a process that allows for much more flexibility in terms of pouch design adjustments. Niiyama et al. attaches a heating element or heat pen to a three-axes CNC stage. They then use the CNC stage to draw the outline of the pouch design by applying pressure to the thermoplastic film with the pen. This process is much more useful for

quick design iterations but does not have large production output potential.

They were able to produce air bladders of various shapes and sizes. They also derive a theoretical model for pouches that are rectangular when deflated. The theoretical model describes the angular and linear modes of pouch actuation. To demonstrate the applicability of the pouch motors, they design a gripper, robotic arm, and locomotive robot. However, the pouches and structures of their robotic systems are manually bonded with adhesives.

1.3 Monolithic fabrication of printable pouch actuators

Recently Zhang, introduced a novel, monolithic printable pouch actuator fabrication method. This method combined fabrication processes of lamination, FDM, and thermal bonding to manufacture pouch actuated robotic systems. The first step of the pouch actuator fabrication is the mask heat pressing process. In order to fabricate the pouches, Zhang laminates two sheets of TPU with a masking layer in between them. The masking layer is a non-heat bondable material that outlines the shape and dimensions of the pouch. Zhang tests a variety of different masking materials and finds water color paint (Mondo Llama) to be the most effective and simple to use. An attachment was designed to attach the paint marker to a 3-d printer to automate the pouch drawing process on the TPU. Once the pouch layout has been drawn in by the 3-d printer, the TPU is removed from the print bed to be heat pressed to the second layer of TPU [13].

Once the pouches are fabricated, they may be placed onto a 3-d print bed for the addition of functional printed top structures. Zhang, also optimized parameters to create an effective bond between the pouches and the 3-d printed structure. Figure1.2 shows a visual representation of the fabrication process. This is the process that is used to design and fabricate the multidirectional prismatic actuators and robot that will be described in the next chapter.

Pouch motors have generally been designed with rectangular shapes. The linear edges of the rectangular shape enables the pouch motor to deform in a more controllable and ”linear” way. However, when fully inflated, the cross section of two perpendicular edges would become a tip

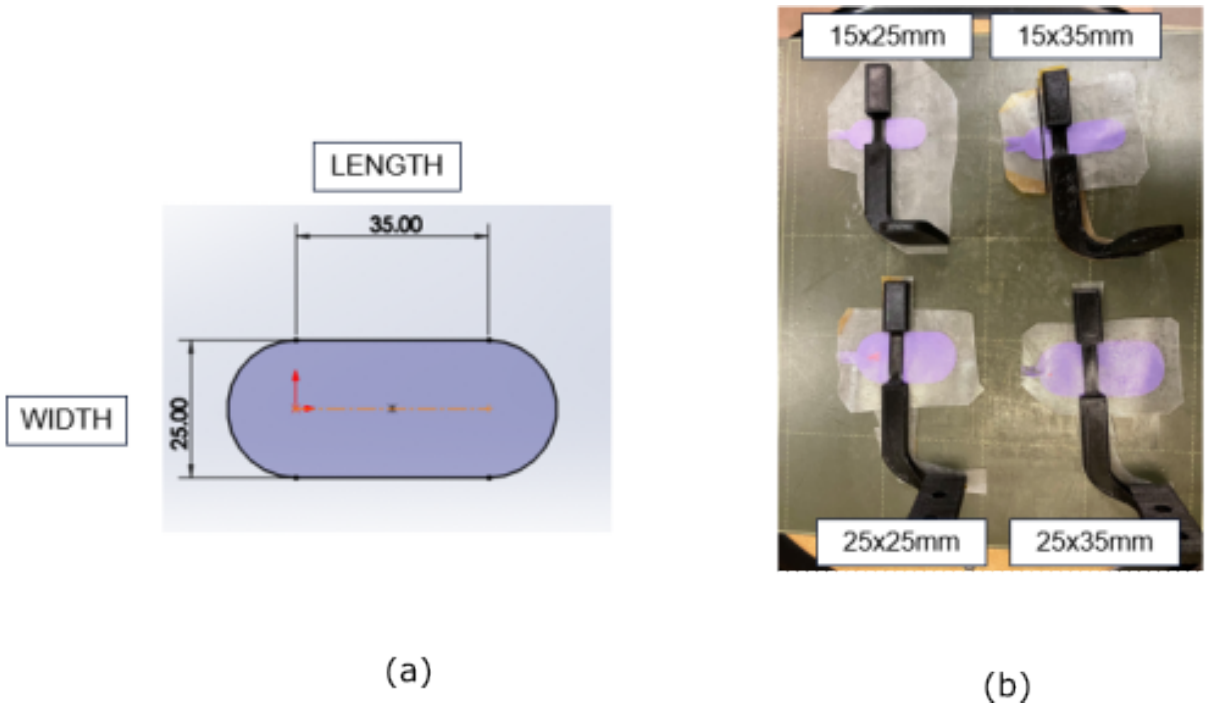

Figure 1.1. a) The naming convention that is used to describe the dimensions of the pouches. b) The different pouch designs that are tested in the rotational performance experiments.

and thus make the linear edges become distorted. For such reason, in this work, all pouch motors were designed in slot shapes. The arcs at both ends would help reduce unwanted deformation and maximize the desired output motions. The distance between the two parallel edges is called width while length refers to the distance from one semi-circle's center to another. The actuator designs will be described using the convention described in Figure 1.1(a) [13].

1.3.1 Monolithically fabricated pouch actuator performance summary

To characterize the performance of the monolithically fabricated pouch actuators, we design an experiment for us to characterize the performance. We focus on measuring the angular displacement and block force output of the four pouch designs shown in Figure1.1 (b). The experimental set up is shown in Figure 1.3. We found that performance of the pouches was more sensitive to width than length. The pouches with larger width had higher angular displacements and block force outputs. Changing the length from 25 mm to 35 mm did not have any conclusive

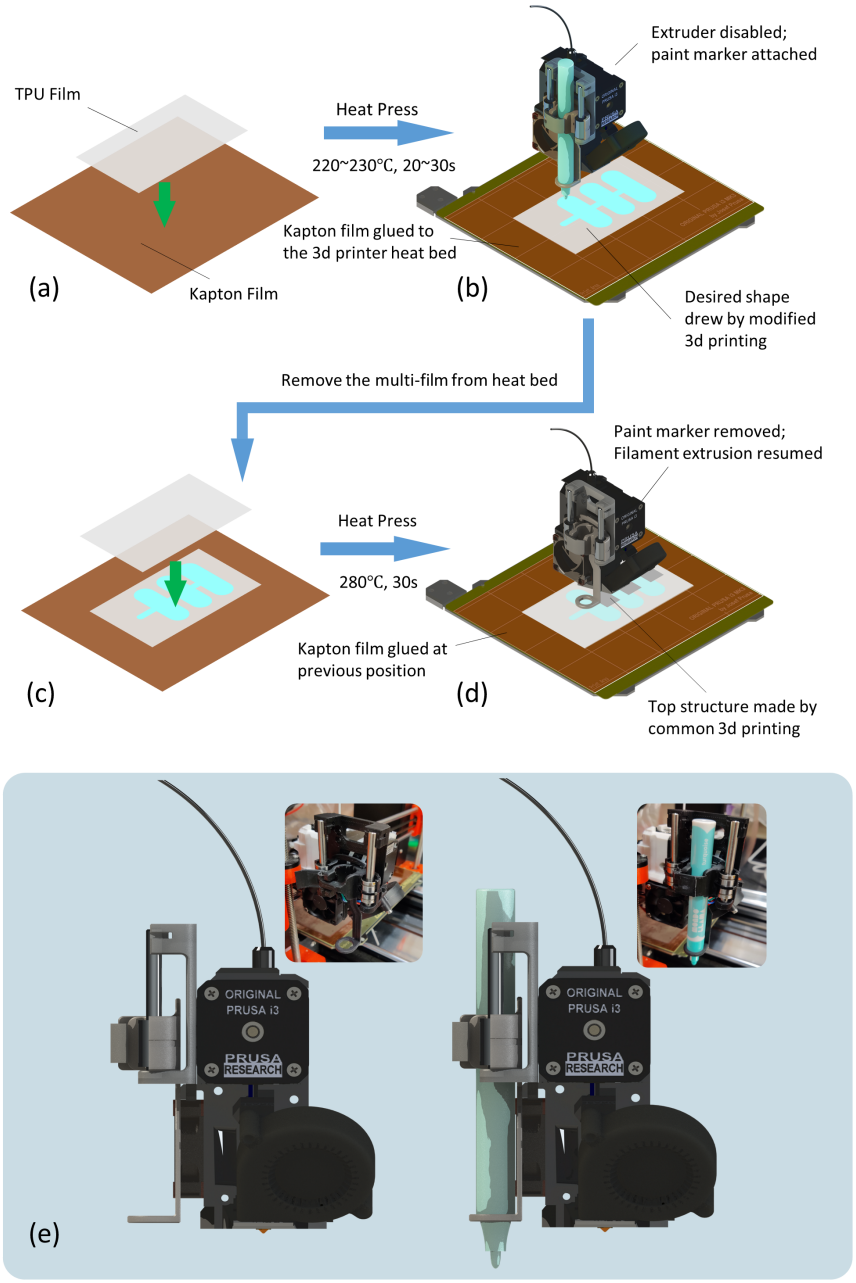

Figure 1.2. (a) Heat press TPU with kapton base film. (b) Plot on TPU film using a paint marker. (c) Heat press another layer of TPU.(d) Resume common 3d printing to create top structures. The whole structure could then be removed from the Kapton base. (e) The 3D printer head attachment is shown

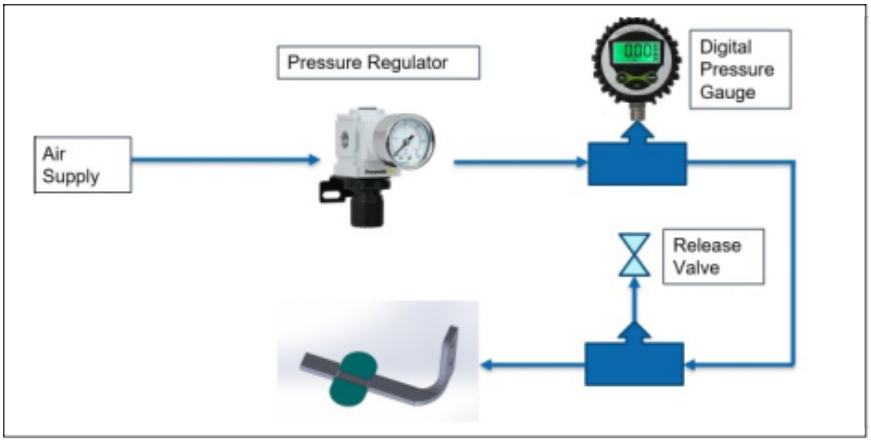

(a)

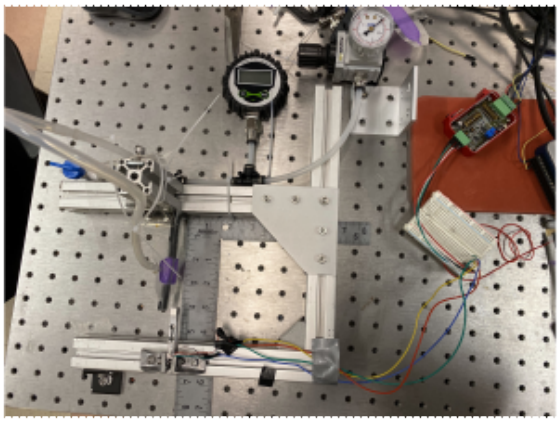

(b)

Figure 1.3. a) The pneuamtic circuit diagram for the experimental set up. b) The actual experimental set up. A load cell is used to measure block force.

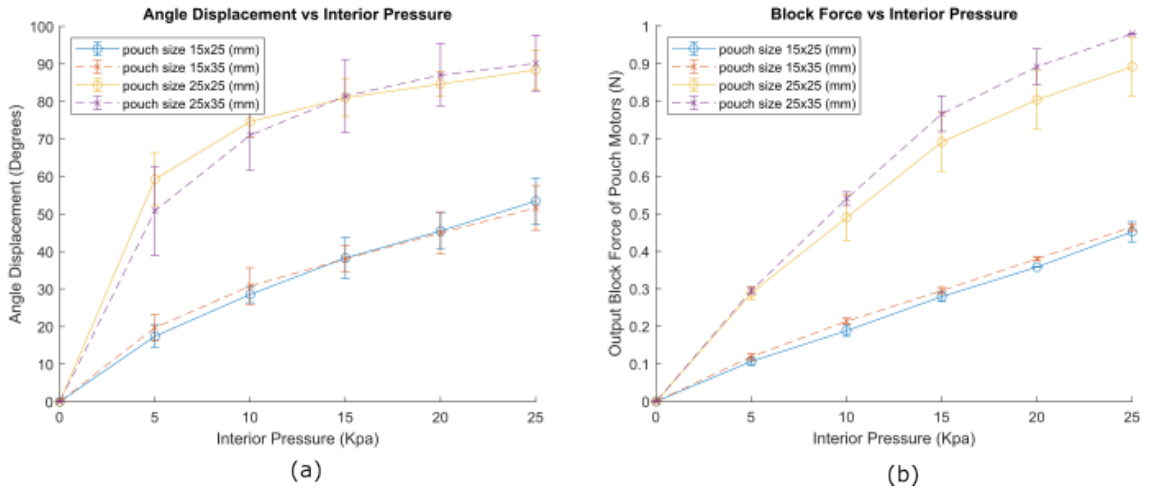

Figure 1.4. a) Angular displacement test results of the four pouch motor samples b) Block force test results of the four pouch motor samples

effects on the performance.

Chapter 1, in part, uses material as it appears in Monolithic Fabrication of Printable Pouch Actuators Shuhang Zhang, Jordan Banh, Nick Gravish. The thesis author is the coauthor of this material.

Chapter 2

Multi-directional motion driven by prismatic pouch actuators

In this section, a system that generates multi-directional motion driven by prismatic pouch actuators will be introduced and tested. Performance will be characterized by angular displacement and block force output. We call this system a multi-directional pouch actuator.

2.1 Multidirectional motion experiments with one fixed pouch surface

2.1.1 Experimental design and setup

Previous work with the mask heat pressed pouch actuators focuses on one-dimensional application of the pouch actuators in the rotational mode. However, these pouches can also be actuated prismatically and be utilized to generate multidirectional motion of a leg. The pouches are laid out in an orthogonal configuration to generate motion in two orthogonal directions, as shown in Figure 2.1. A 3D printed leg is attached to the pouches via a snap-fit hinge. The snap-fit hinge is directly printed onto the pouch using the fabrication process from the monolithic pouch fabrication process described in the previous section. The joints that are above the pouches will be treated as a rotational joint and any off-axis rotation will not be considered. The appendage is also connected to the ground plane via a snap in socket. This particular connection will be treated as a ball joint. Due to clearances in the design, the leg can travel ±1 mm along the z-axis

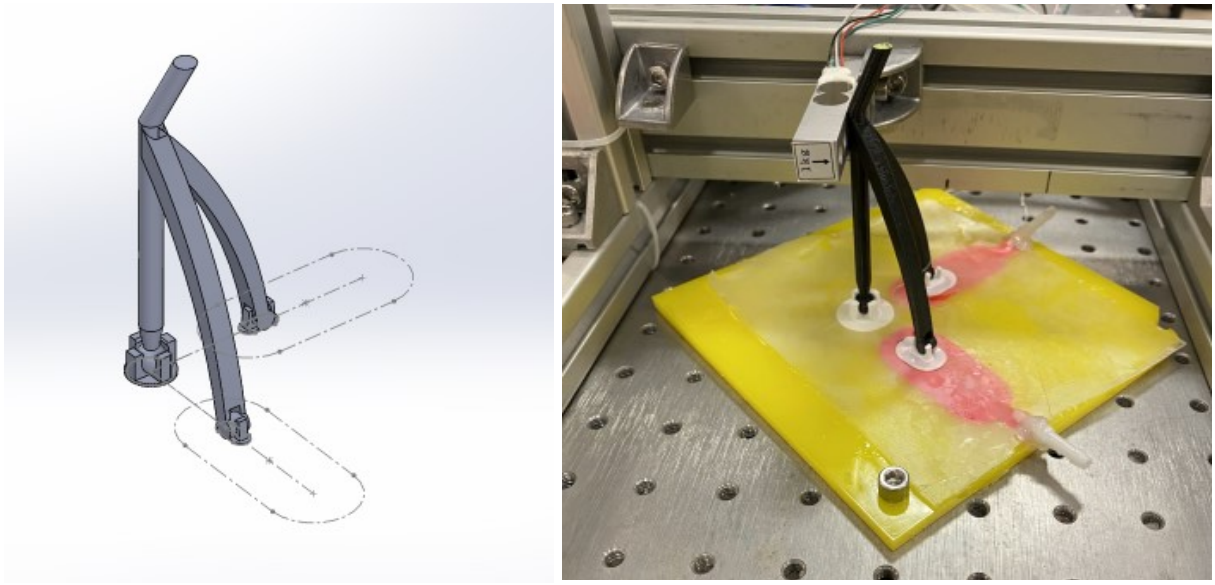

Figure 2.1. a) The multi-directional pouch actuator design is shown. The z-axis is defined as the line orthogonal to both pouch axes (along the length of the pouch). b) The experimental set up is shown. A load cell is placed perpendicular to the expected direction of motion to measure block force.

but this effect will not be considered in the experiment. In the previous section, 25mm x 35mm pouches were shown to exert the largest amount of force and angular deflection in the rotational mode. This can be attributed to the larger amount of surface area that the air pressure acts on. For this reason, a 25 mm width pouch is chosen for the prismatic actuator experiments. The geometry of the 25 mm pouch design should also lead to the greatest amount of z-displacement when inflated. The length of the pouch is 35 mm. Previous experiments, show that the width has dominant effects on the performance of the pouch so the length of the pouch should not an important design variable [13]. After the pouches are fabricated, the pouches are fixed to an acrylic plate using epoxy.

The performance of the multi-directional actuator will be characterized by angular displacement and block force output experiments. The same pneumatic circuit in Figure 1.3(a) is used. The measurements and results are discussed in the following sections. The goal of these experiments is to understand if there are any significant differences in performance during

one-pouch inflation and two-pouch inflation. The same 3D printed leg is used for all experiments. For each multi-directional pouch, the angular displacement and block force are measured three times for each increment of pressure. Then we calculate the average and standard deviation for the measurements for the three different multi-directional pouches.

Angular deflection

To measure the angular displacement from singular pouch inflation, we measure from the vertical axis to the center axis of the appendage within the expected plane of motion. The expected plane of motion is defined by the z-axis and the axis along the pouch which is being actuated. The pouch will be inflated from an interior pressure 0 kPa to 25 kPa in increments of 5 kPa. The pouches are not inflated above 25 kPa to avoid delamination. A photo will be taken at each increment and measured using an image processing software. An example of the photos is shown in 2.2(a).

For the two pouch configuration, the plane of motion will be be defined by the line of equality (where the pouch axes are defined as the x- and y- axes) and the vertical axis. Both pouches are inflated from 0 Kpa to 25 Kpa in increments of 5 Kpa. The angle is measured using a photo and image processing as well. An example of the photo is shown. 2.2 (b)

Using CAD software, we simulated angular deflection when the pouch raises the hinge 7 mm. To simplify the simulation, we simplified the rolling joint geometry to a point that is free to rotate. The simulation showed that one pouch inflation led to an angular deflection of 3.9 degrees. The simulation for two pouch inflation showed and angular deflection of 3.2 degrees. Therefore, we expect our experimental results to show that one pouch inflation will lead to greater deflection than that of the two pouch inflation.

Block force setup

The block force output measurement procedure is similar to that of the angular deflection measurements. First, a load cell is fixed at the location of the tip of the leg which is 70mm from

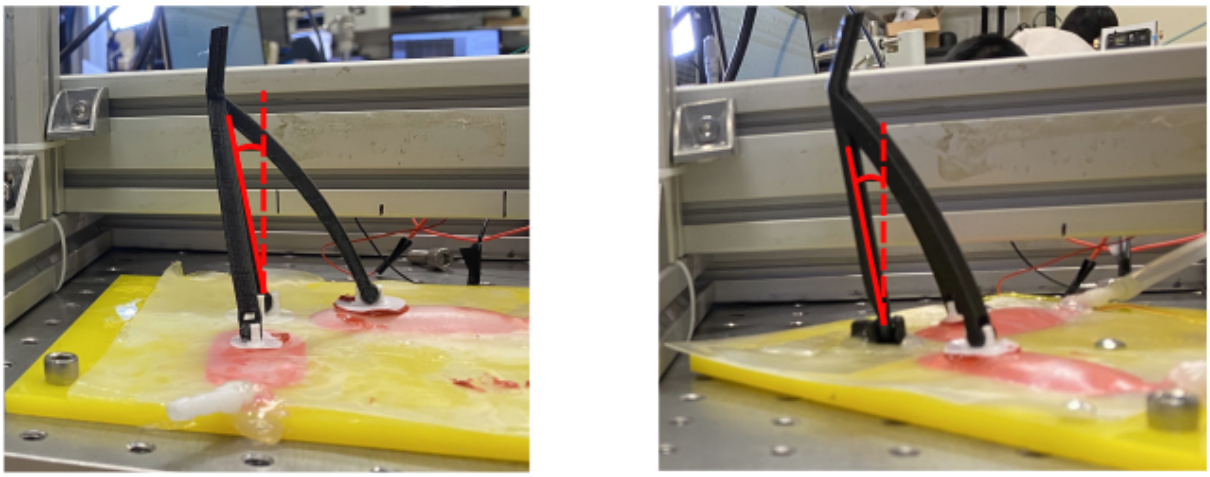

Figure 2.2. a)An example of how angular displacement is measured for one pouch inflation. b) An example of how angular displacement is measured for two pouch inflation.

the acrylic plane. Then a single pouch will be inflated from an interior pressure 0 Kpa to 25 Kpa in increments of 5 Kpa; the block force is measured at each increment. Then the procedure is repeated with two pouch inflation. We expect to see an increased block force output for the two pouch actuation because there will be a larger effective surface area that the interior pressure of the pouches will be applied on.

2.1.2 Results

Results of the angular displacement and block force experiments are shown in Figure 2.3. The angular displacement tests show that there is a clear performance increase when using the two-pouch inflation. This contradicts the results from our simulation. The disparity is likely due to the clearances in the design. The 3D printed ball joint is not perfectly fixed at a point in space and will cause a disparity between reality and simulation. The rotational joints are also not perfectly aligned along the pouch axes. Any off-axis rotation at the rotational joints will also have an effect on the rotational displacement measurements.

However, for the block force experiment there is no clear performance difference between the one-pouch inflation and two pouch inflation. The data shows that the block force for two

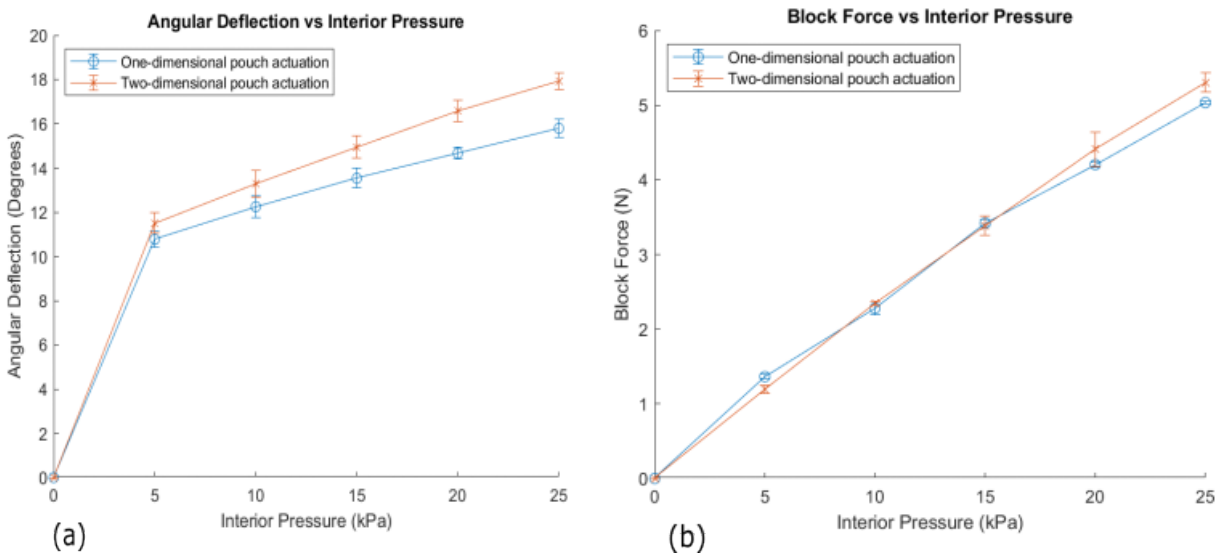

Figure 2.3. a) Angular Deflection test results for one-dimensional pouch actuation and two-dimensional pouch actuation b) Block force test results for one-dimensional pouch actuation and two-dimensional pouch actuation

pouch inflation is slightly greater when the interior pressure is greater than 15 kPa, but the difference is not great enough to make a definitive conclusion. The multi-directional pouch actuator can exert up to 5.03 ±0.1 N of force when one pouch is pressurized. Up to 5.3 ±0.1 N of force can be exerted when pressurizing two pouches.

2.2 Rigid vs. free surface

When the pouch actuators are being integrated into a robotic system, the pouch actuators may not always be fixed to a rigid surface. For this reason, it is important to understand how this may affect pouch performance. To further understand the performance of the pouch actuators, we design an experiment to analyze whether there is a performance difference when both sides of the pouches are free surfaces or if one side of the pouch is fixed. This section explains the experimental set up and results. We expect that block force output may decrease because the reaction forces may cause the pouch to deflect in the negative z-direction. Energy will be lost in the elastic deformation of the TPU sheets. We do not expect there to be a performance difference for the angular displacement experiments because there should not be significant reaction forces

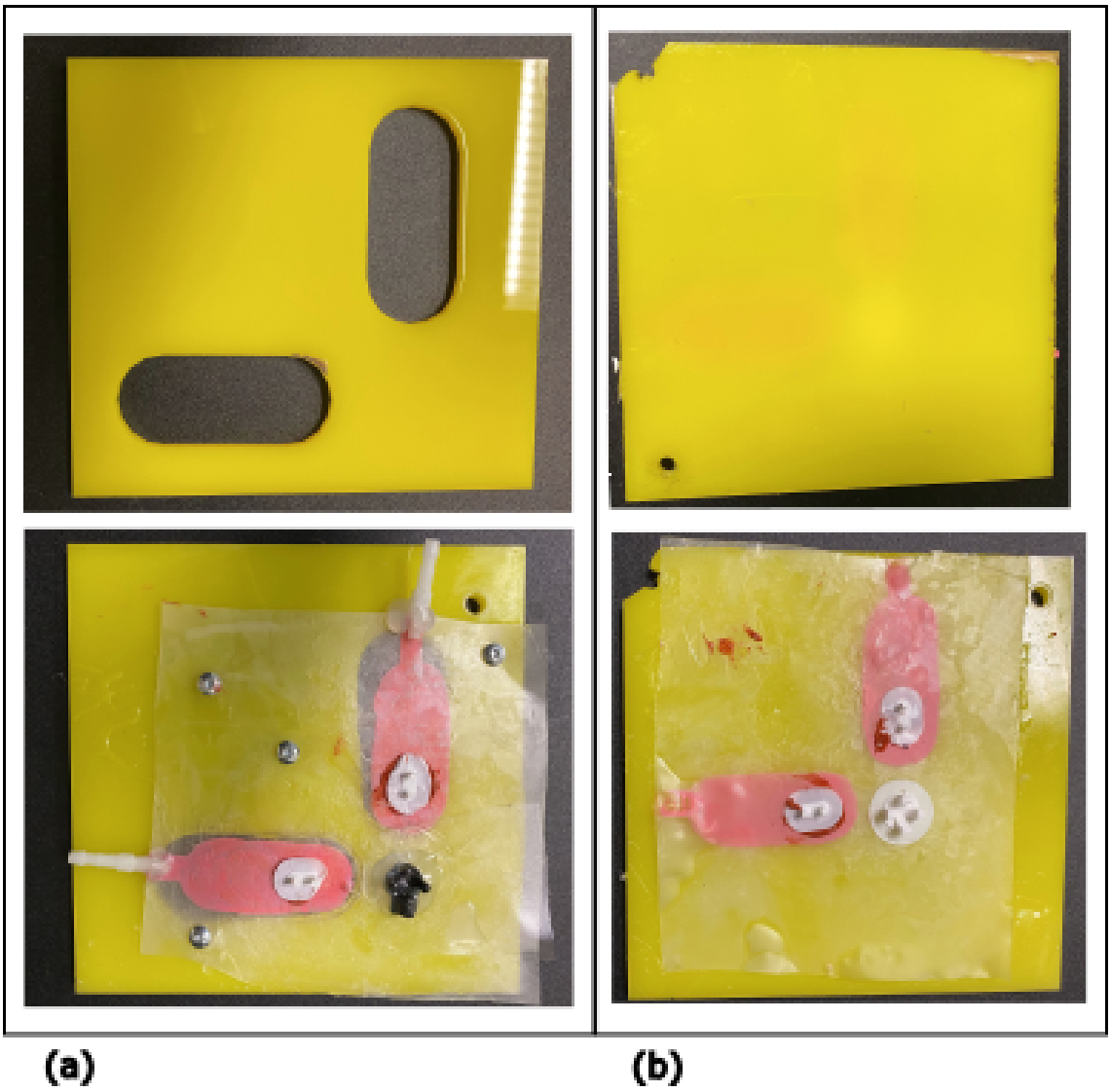

Figure 2.4. a) A photo of the acrylic sheet with cutouts is shown on top. The bottom photo shows the pouches that are fixed to the acrylic sheet. The sheet is fixed using epoxy. b) The top photo shows a flat acrylic sheet. The bottom photo shows the pouches that are fixed to the flat acrylic sheet using epoxy.

at the tip of the leg. Therefore, the pouches will not deflect in the negative z-direction and energy will not be lost through elastic deformation.

2.2.1 Experimental Set-Up

The pouch layout and design specifications from the previous experiment are used. We fabricate two sets of pouches. We fix one set of pouches to an acrylic sheet with cutouts that outline the shape of the pouches. As shown in Figure 2.4 (a) the cutout dimensions are offset from the pouch dimensions by 5 cm. The other set of pouches is simply fixed to a flat acrylic sheet using epoxy (shown in Figure 2.4 (b)) The angular and block force measurements are taken using the procedure mentioned in the previous experiment.

2.2.2 Results

Figure 2.5 (a) shows the results from the angular deflection experiment. The set of pouches fixed to an acrylic surface and set of pouches with a free surface maintain the angular displacement trends found in the previous experiments: two-dimensional pouch actuation leads to greater angular deflection. However, the pouches that are free on both sides have lower angular deflections than that of the sets of pouches with a fixed surface. There is also a clear decrease in the block force for the sets of pouches with free surfaces. Singular pouch inflation block force is also significantly lower than that of the two-pouch inflation. This is likely because the deflection of the TPU sheets in the negative z-direction is only affecting one pouch as opposed to two. The two-pouch configuration has larger amounts of TPU material that is able to resist the elastic deformation.

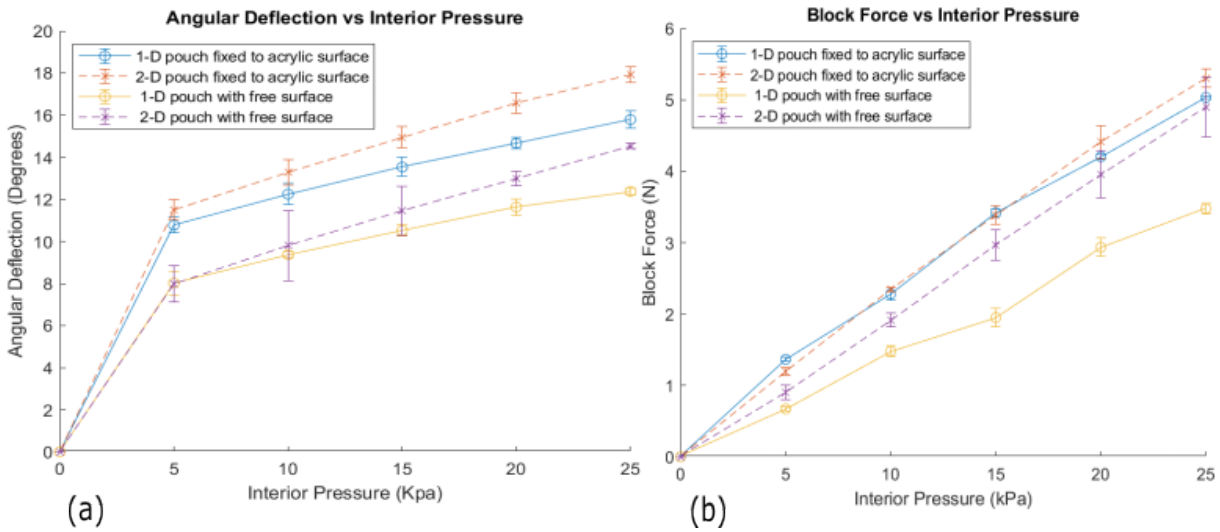

Figure 2.5. a) Angular deflection test results for one-dimensional pouch actuation and two dimensional pouch actuation b) Block force test results for one-dimensional pouch actuation and two-dimensional pouch actuation

Chapter 3

Locomotive robot design, fabrication and Tests

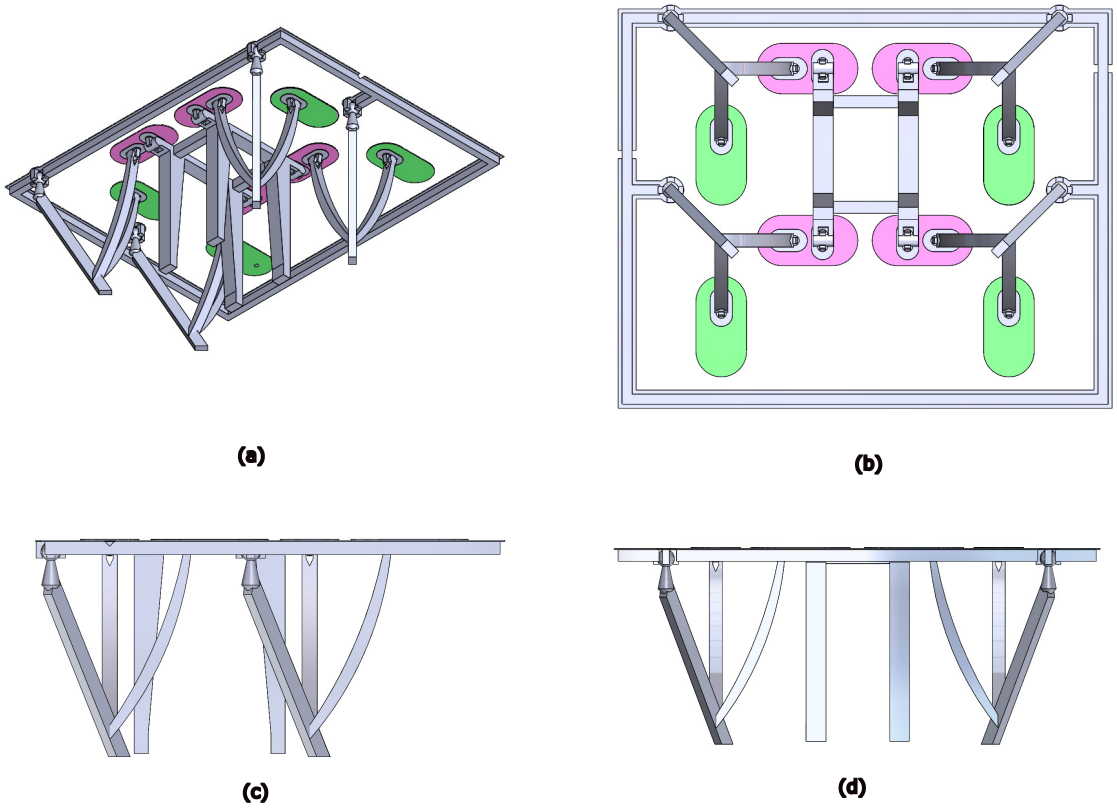

Figure 3.1. Robot Design a) Isometric view. The outer legs and inner legs can be seen here b) Bottom view. Green pouches control longitudinal motion. Pink pouches control lateral motion of the outer legs. The pink pouches also control motion along the z-axis for the inner leg. c) Side view d) Front view

3.1 Locomotive robot design

Our next goal was to utilize these multi-directional prismatic pouch actuators for locomotion. We have previously proven that the pouch actuators can general multi-directional motion and exert up to 5 N of force. The robot design includes four of the multi-directional actuation systems that are similar to that of the previous experiments. Modifications were made to the position of the ball joint and the shape of the leg. The leg design is modified so the foot would have greater displacement along the z-direction. These four legs are placed near the perimeter of the robot and are referred to as the outer legs. Another leg was also designed to generate greater z-displacement so the outer legs could achieve a clear swing phase; this leg will be referred to as the inner leg. The inner leg is actuated by the latitudinal pouches, at the center of all the outer legs. Figure 3.1 (a) shows the robot design.

The pouch fabrication process allows us to embed channels into the robot design and couple the actuation of the pouches. We grouped the latitudinal pouches and longitudinal pouches separately. In other words, the inflation of the latitudinal pouches are coupled and the inflation of the longitudinal pouches are coupled. Since the latitudinal and longitudinal pouches are grouped separately, we only need 2 valves to control the robot. The longitudinal pouches actuate the outer legs in the longitudinal direction; the latitudinal pouches actuate the outer legs in the latitudinal direction. The latitudinal pouches also generate inner leg motion along the z-axis. See Figure 3.1(b)

In the previous section, we showed that pouches that are fixed to a rigid surface have performance improvements when compared to that of the pouches with two free surfaces. For this reason, we fix a rigid sheet of FR4 to the top side of the robot using epoxy. We also 3-d printed a rectangular structure around the border of the robot to increase rigidity.

An air compressor provides 35 kPa of supply pressure to inflate the pouches. We use mini valves to control the inflation and deflation of the pouches. The configuration of the pouches is shown in Figure 3.2. Tube fittings are attached to the channels outlets of the robot using hot glue.

Tubes coming from the valves are connected to the tube fittings.

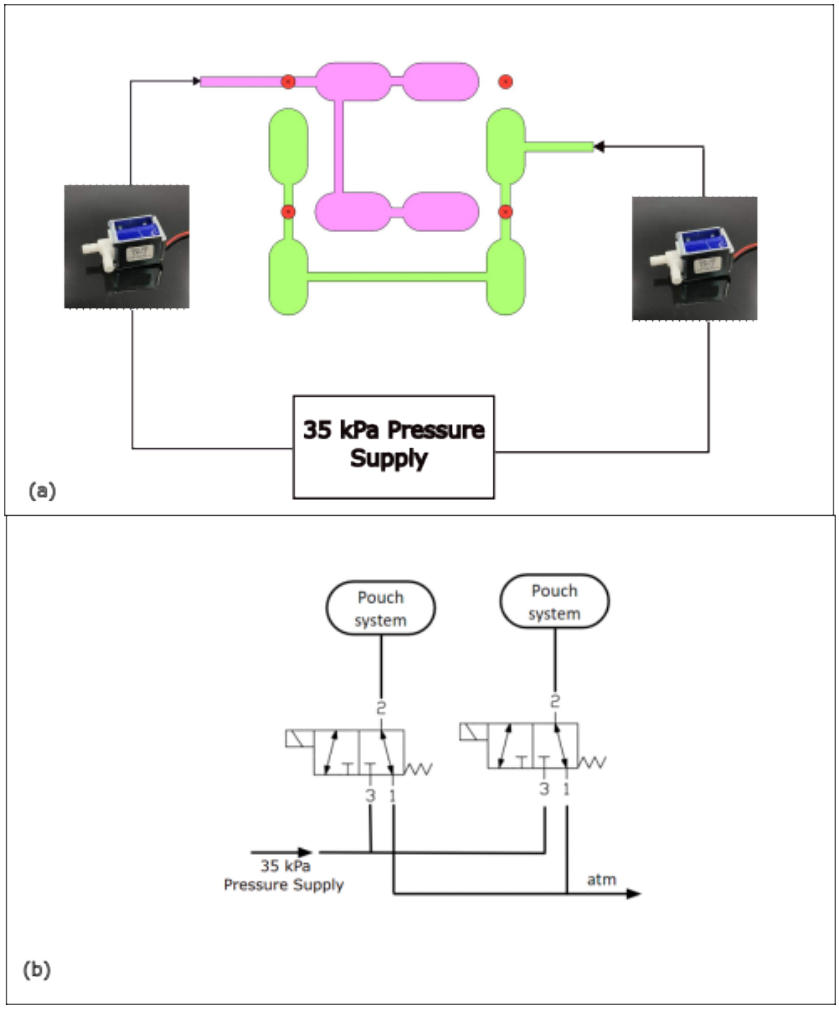

Figure 3.2. a) This photo shows the layout of the pouches and valves. The pink pouches are defined as the latitudinal pouches and the green pouches are defined as longitudinal pouches.The red circles represent the home position of the robot feet when the pouches are deflated. b) The pneumatic circuit is shown

3.2 Gait cycle

The gait cycle is organized into four different steps. Figure 3.3 and shows locomotion gait cycle in the positive x-direction.

In the first phase of the gait sequence, the pink pouches are pressurized. The pink pouches actuate the outer legs in the lateral direction. Due to the geometry of the leg and location of the ball joint, the outer feet are also slightly displaced in the negative z-direction. The pink pouches also actuate the inner leg towards the negative z-direction. This leads the inner leg to lift the rest of the robot chassis in the positive z-direction. At this point, the outer legs are suspended in air by a few millimeters.

Then the longitudinal pouches are pressurized. This leads the outer legs to move in positive x-direction. The foot also moves in the negative z-direction. This part of the motion sequence can be seen as the swing phase of the gait sequence.

In the third step, the pink pouches are deflated and this realigns the outer feet along the longitudinal pouch axes. The inner leg is also lifted in the positive z-direction. This leads the robot chassis to lower itself in the negative z-direction. At this point in time the inner leg is suspended in air while the robot is being supported by the outer legs.

In the final step of the sequence, the longitudinal pouches are depressurized. This leads the outer legs to exert force in the negative x-direction and move the robot chassis forward. The robot chassis is supported by all five legs in this phase.

For the locomotion in the negative x-direction, the entire process is reversed.

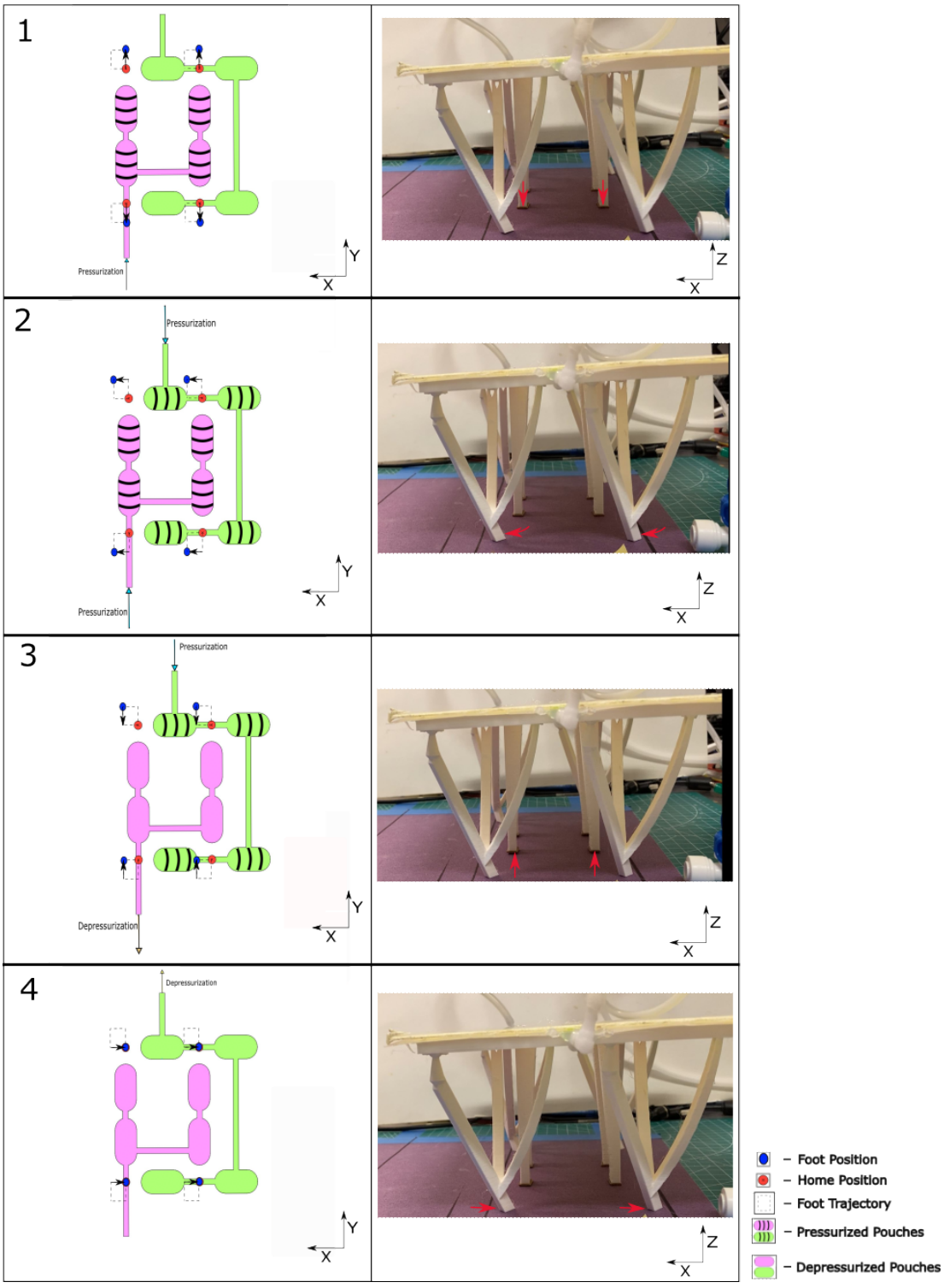

Figure 3.3. The locomotion gait in the positive x-direction is shown. The red arrows represent the motion of the feet projected onto the x-z plane.

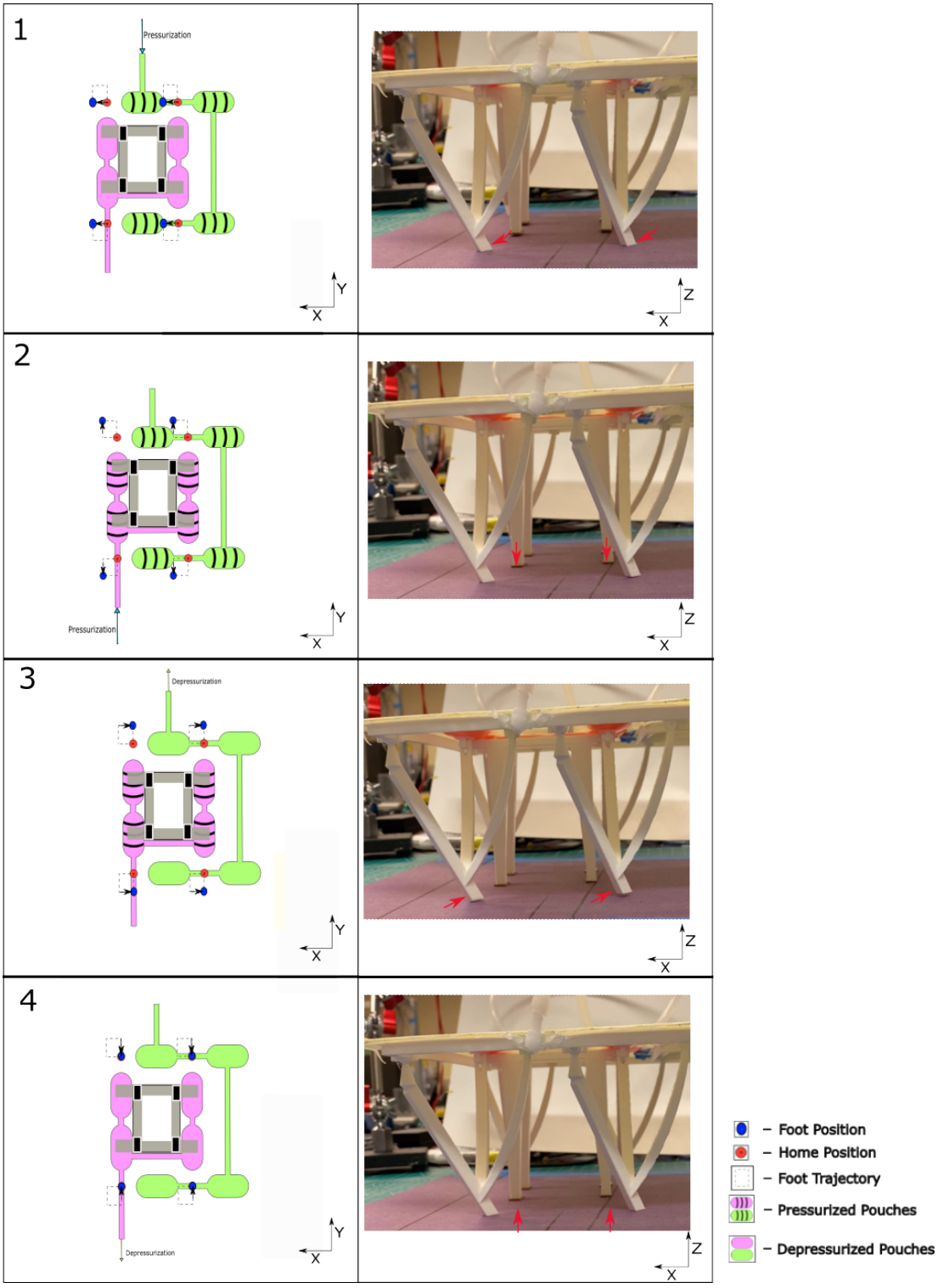

Figure 3.4. The locomotion gait in the negative x-direction is shown.

3.3 Performance Experiments

Our first test measures the speed of the robot locomotion at different cycle frequencies. The cycle frequency is determined by the length of the delays between each step of the gait sequence. The length of the delay is constant for each frequency. We take speed measurements of the robot in the positive and negative x-direction. For each frequency, we record the time it takes the robot to walk 100 mm and calculate the speed. We take 3 measurements for each frequency for locomotion in the positive and negative x-direction. The average and standard deviation are taken for each the measurements at each frequency for each direction. A 35 kPa pressure supply is used for this experiment.

The second experiment measures the ideal distance gained at each cycle frequency (defined as L). Ideal distance gained is defined as the horizontal travel of the foot from longitudinal pouch inflation to deflation during steady state. We measured the free displacement of the outer leg by placing a robot on a pedestal that only contacts the inner leg (shown in Figure 3.5). This allows the outer legs to move freely. A 35 kPa pressure supply is used for this experiment.

There may be some performance loss from the limitations of the valve exhaustion. The valve exhaustion rate may not be able to keep up with the rate of pouch deflation. Since the pouch deflation is passive, the pouch may not be able to fully deflate before the pouch begins inflating again. The rate of deflation decreases as the pressure difference between the pouch interior and atmosphere decreases. We wanted to understand how this affects the ideal distance gained at each cycle frequency. We expect to see a decrease in the ideal distance gained as cycle frequency increases. The maximum range of motion is defined as the amount of horizontal travel at 0 Hz cycle frequency. The ideal distance gained per cycle (ideal L) is measured from the start of before and after the longitudinal pouch inflation during steady state. A picture is taken before and after longitudinal pouch inflation and then the horizontal displacement is measured using a ruler that is placed below the outer foot. An example of the photo taken and the measurement is shown in Figure 3.5. The actual distance gained, defined as the actual L, is calculated from the

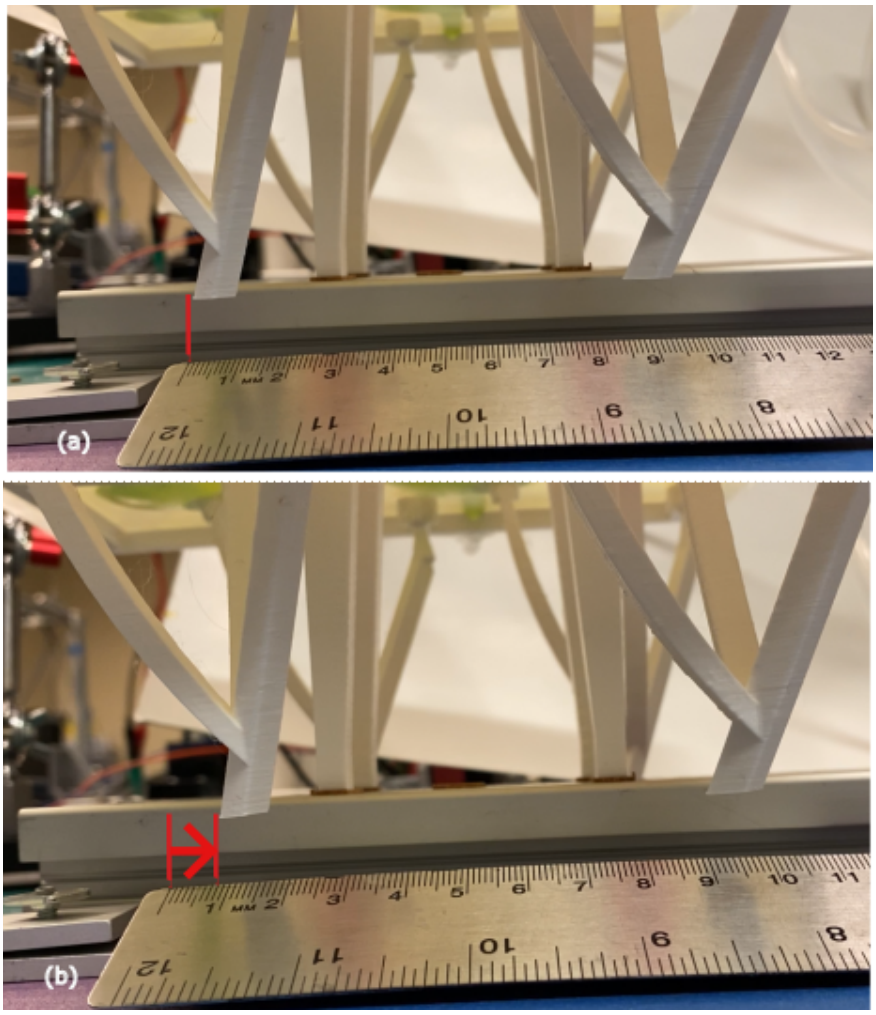

Figure 3.5. a) A photo of the outer leg before longitudinal pouch inflation b) A photo of the outer leg after longitudinal pouch inflation.

data obtained in the speed versus frequency experiments. We can calculate the amount of actual distance gained per cycle by dividing speed by frequency. We also tested how the robot would perform carrying different payloads. We maintained a cycle frequency of 0.25 Hz because in the previous experiments, we learned that the robot is able to maintain speed and distance gained per cycle at this frequency. At frequencies of 0.25 Hz, there is enough time for the pouches to deflate. We increased the payload in increments of 250 grams until failure. Failure is defined to be the point at which the robot is no longer able to walk. The payload is placed on the top surface of the robot, above the center of gravity. A 35 kPa pressure supply is used for this experiment.

3.4 Results

There is a linear increase in speed as cycle frequency increases from 0.83Hz to 0.25Hz. However, as the cycle frequency increases beyond 0.25 Hz the speed increases at a lower rate. There is a divergence in performance for locomotion in the positive and negative x-direction. Locomotion in the negative direction becomes significantly slower when compared to locomotion in the positive x-direction. There is a large decrease in speed when cycle frequency is 0.83 Hz.

For locomotion in the negative x-direction , the robot is able to maintain an increase in speed until cycle frequency is increased to 0.83 Hz. However, the robot is unable to achieve locomotion in both directions when the cycle frequency is 1.25 Hz.

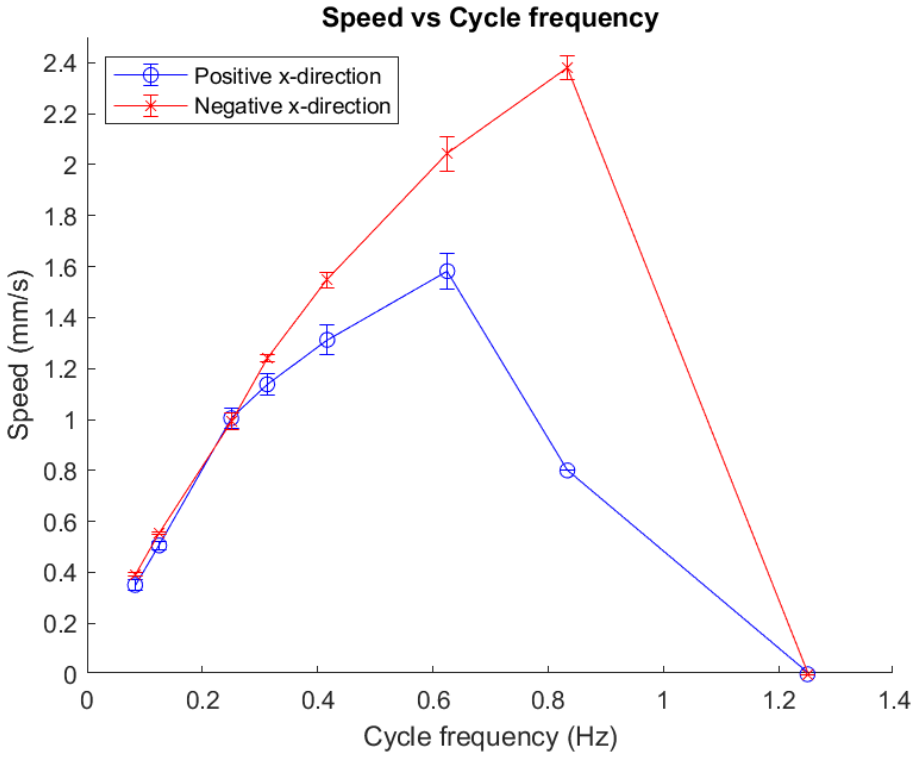

Figure 3.6. a) Speed (mm/s) versus Cycle frequency (Hz). Locomotion in the negative direction (denoted by red) is faster when the frequency is increased beyond 0.25 Hz. The robot can not achieve locomotion at frequencies greater than 1.25 Hz.

As frequency increases, the ideal distance gained per cycle linearly decreases from 8.0 mm to 4.2 mm. The actual L in the positive direction is consistently lower than that of the

negative x-direction. For the positive x-direction, the distance lost is 3.5 ±0.5 mm. For the negative x-direction, the distance lost is 2.9 ±0.6 mm. For both cases, the dominant contributing factor is slipping. Another contributing factor is the geometry of the robot design. There are times when the outer legs are unable to complete a full leg swing due to interference with the ground. The design can be tuned and optimized to decrease the distance lost.

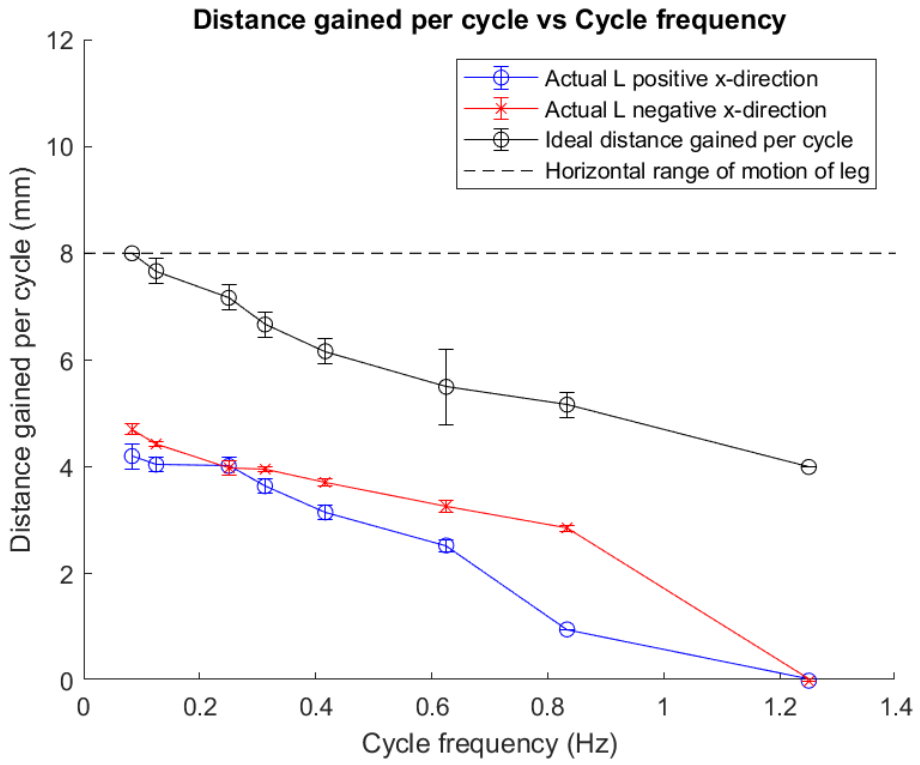

Figure 3.7. a) Results from the distance gained per cycle experiment. Horizontal range of motion of the leg is 8mm. The ideal distance gained (black) decreases as frequency increases. The actual L is less than the ideal L. L in the positive x-direction is less than that of the negative x-direction

As payload increases, the speed decreases. A contributing factor to this is that as the payload increases, the z-displacement of the inner leg also decreases. This affects the swing phase of the outer legs and increases the amount of interference with the ground during the swing phase. The robot is able to reliably carry up to 1250 grams of payload.

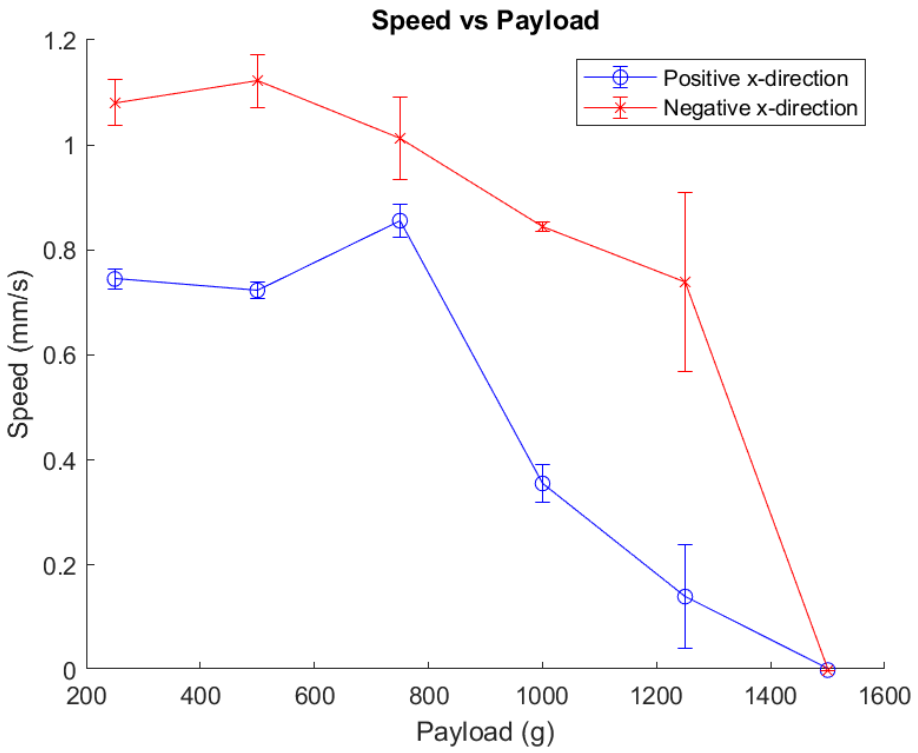

Figure 3.8. a) Locomotion speed of robot with different payloads. The robot is able to carry payloads up to 1250 grams reliably.

3.5 Summary

As cycle frequency increases, locomotion speed in the positive and negative direction increases. At cycle frequencies above 0.25 Hz, locomotion speed in the negative x-direction is greater than that of the positive x-direction. As cycle frequency increases, the distance of the horizontal travel of the foot decreases. The robot is able to reliably carry payloads that are 4.4 times the transmission weight. However, as payload increases, speed of the robot decreases.

Chapter 4

Locomotive robot demonstrations

4.1 Untethered robot locomotion

4.1.1 Untethered system and control

The untethered onboard system is shown in the Figure 4.1. Two mini valves are controlled by an Arduino Uno which is powered by its own battery. An onboard mini pump is powered by a separate battery. The untethered system and robot chassis weighs 500 grams. We demonstrated untethered locomotion over a distance in positive and negative x-direction. We also demonstrated locomotion over 200 mm in the negative x-direction in Figure 4.2. Due to uneven ground and imperfections in the robot fabrication, the robot did not move in a perfectly straight line.

4.2 Robot capable of bidirectional locomotion

4.2.1 Design

After studying locomotion along the x-direction, we designed a robot that is also capable of locomotion in the positive and negative y-direction. The pouch layout is very similar to that of the previous robot design. The first modification that we made is decoupling actuation in the vertical direction and y-direction. We also decoupled the actuation in the positive and negative y-direction. We now have four different pouch groupings; each group is controlled by an independent valve. The latitudinal pouches that control the legs that are farther along the

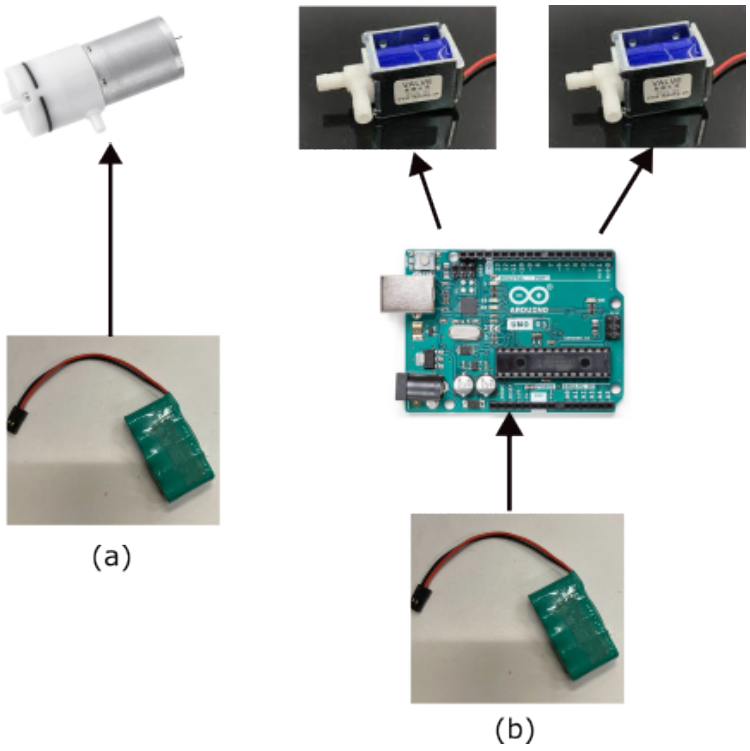

Figure 4.1. a) The pump is powered by an independent battery. b) The Arduino Uno and valves are powered by an independent battery. The Arduino Uno controls the mode of the valves.

y-axis will be called the starboard pouches. The pouches that are closer to the x-axis will be called the portside pouches

4.2.2 Gait cycle

The gait in Figure 4.4 shows the robot walking in the positive y-direction. The first phase in the gait cycle actuates the pouches that control the inner leg. This pushes the inner leg downwards and lifts the outer legs off the ground. Then the outer legs that are farther along the positive y-axis swing outwards, in the positive y-direction. Then the inner pouches deflate and the outer legs support the robot. In this stage, the portside pouches are deflated and the starboard pouches are inflated. This leads the robot chassis to move in the positive y-direction.

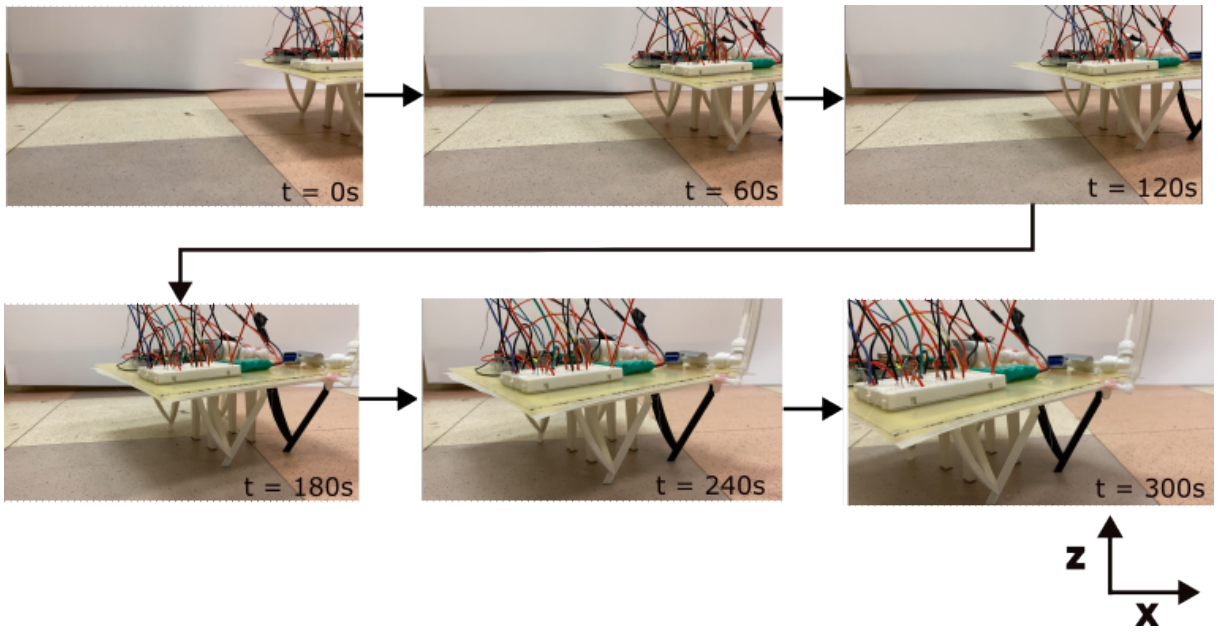

Figure 4.2. a) The untethererd robot traveled over 200 mm in the negative x-direction.

4.2.3 Demonstration

Ultimately, we demonstrate the robots capability to walk in the latitudinal direction (shown in Figure 4.5) as well as the longitudinal direction.

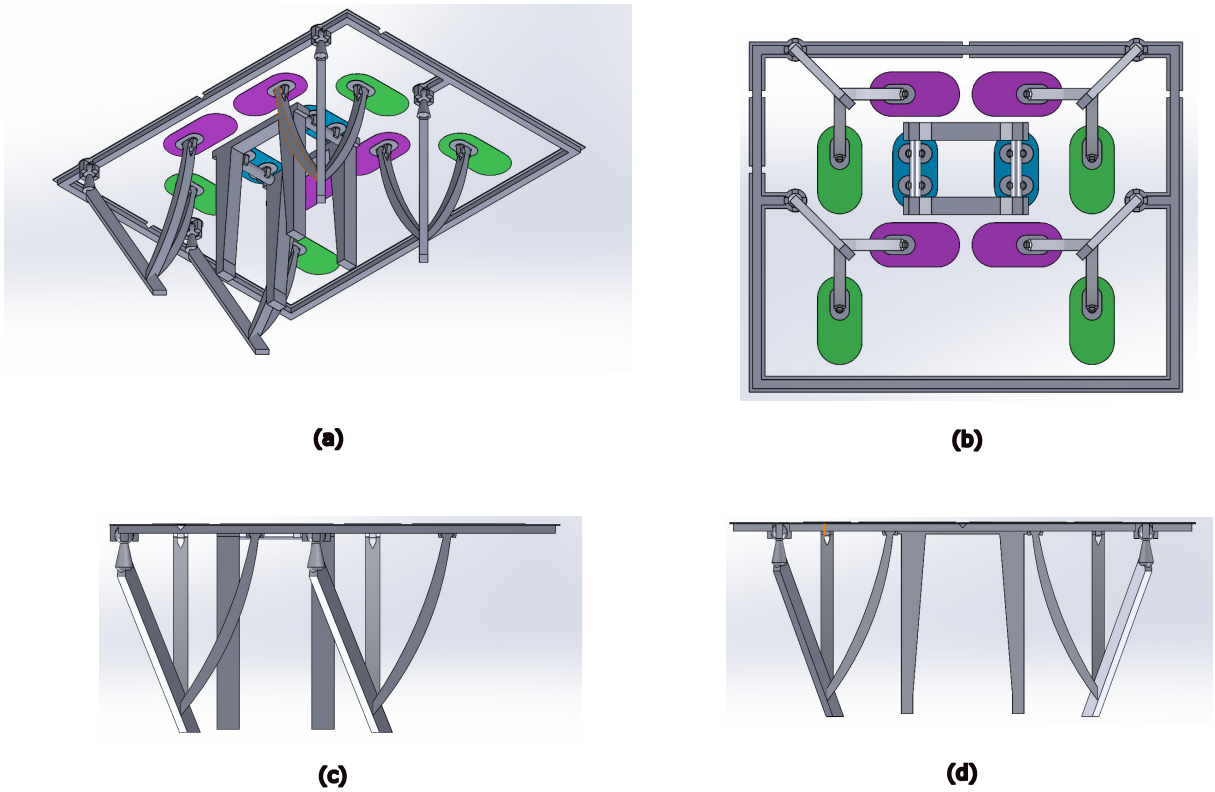

Figure 4.3. a) Bi-directional locomotive robot design

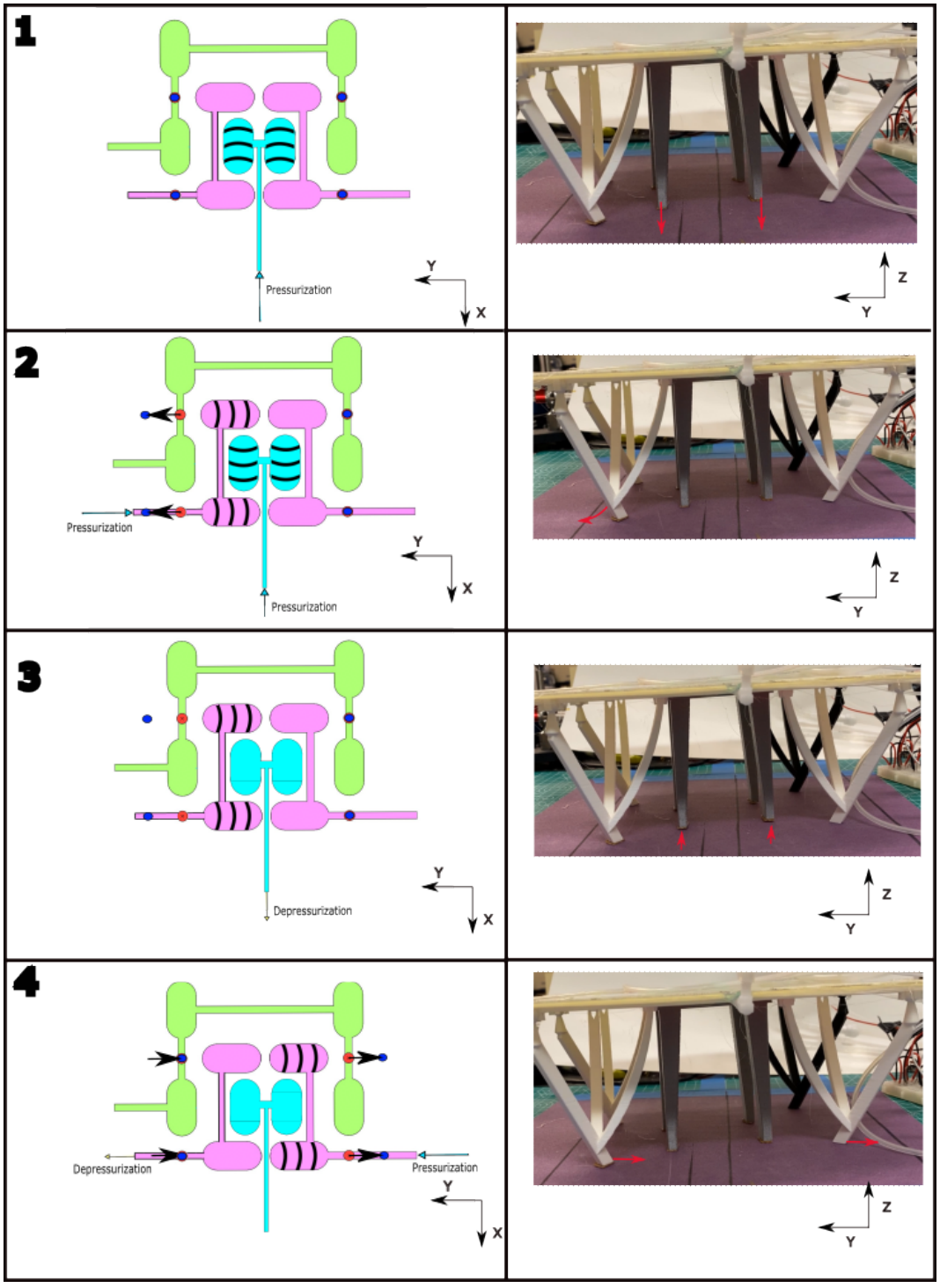

Figure 4.4. Locomotion in the positive y-direction.

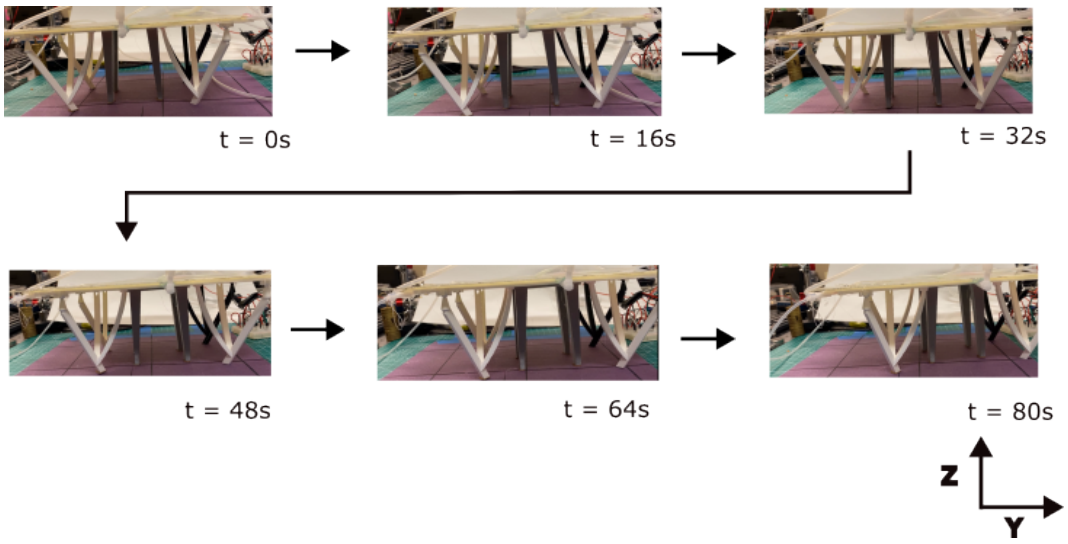

Figure 4.5. Locomotion in the latiudinal direction

Chapter 5

Conclusion and future works

5.1 Conclusion

In this work, we analyzed the prismatic mode of pouch actuators. We utilized these prismatic actuators to generate multi-directional motion and force. For angular displacement, two-pouch actuation generated larger angular displacements than that of the one-pouch actuation. There was not a distinct difference in block force output when using one pouch or two pouches. Then we found that fixing the pouches to a rigid surface improved the performance of the multi-directional pouch actuators.

Finally, we utilized these pouch actuators in the design of a locomotive robot. The robot walks faster in the negative x-direction at higher frequencies. At higher frequencies, the robot walks less efficiently due to the limitations of valve exhaustion and nature of pouch deflation. We also demonstrated that the robot is able to reliably carry 4.4 times the chassis weight. After testing, we demonstrated that the robot can be easily modified to be untethered pneumatically and electronically. We also demonstrated that the robot can be designed to walk laterally and longitudinally.

Unfortunately, this robot would not perform well in large open environments with obstacles. This robot will excel in large open environments with level ground. Since the robot chassis maintains a level surface during locomotion, payloads can be placed on top of the robot with out the need to be securely fastened. This robot could potentially be used in robot-human

collaborative environments such as warehouses where it can be used to carry heavy loads in a controlled, level environment. This robot also uses fabrication processes and materials that are easily accessible. The fabrication process and assembly of the robot is relatively simple and easy to control.

5.2 Future Works

This robot can already carry a significant payload, but increasing the number of legs and pouches would likely improve the robot performance in this regard. Using the monolithic fabrication method, we can manufacture a large number of multidirectional pouch actuators very quickly. Adding more legs would also likely improve the stability of the robot. Using this monolithic fabrication method, we could also design channels that take advantage of fluid viscosity to generate inherent time delayed actuation. This would allow us to have extremely simplified control systems and reduce electronic components.

Future work would also include the optimization of the robot locomotion. The design of the legs and the robot can be adjusted to reduce slipping. Also, increasing the amount of inner legs that actuate in the z-direction would likely increase the amount of mass that the robot can carry.

Bibliography

[1] Eric Brown et al. “Universal robotic gripper based on the jamming of granular material”. In: *Proceedings of the National Academy of Sciences* 107.44 (2010), pp. 18809–18814. DOI: 10.1073/pnas.1003250107. eprint: https://www.pnas.org/doi/pdf/10.1073/pnas.1003250107. URL: https://www.pnas.org/doi/abs/10.1073/pnas.1003250107.

[2] M. Calisti, G. Picardi, and C. Laschi. “Fundamentals of Soft Robot locomotion”. In: *Journal of The Royal Society Interface* 14.130 (2017), p. 20170101. DOI: 10.1098/rsif.2017.0101.

[3] Jorge G. Cham et al. “Fast and Robust: Hexapedal Robots via Shape Deposition Manufacturing”. In: *The International Journal of Robotics Research* 21.10-11 (2002), pp. 869–882. DOI: 10.1177/0278364902021010837. eprint: https://doi.org/10.1177/0278364902021010837. URL: https://doi.org/10.1177/0278364902021010837.

[4] Sangbae Kim, Cecilia Laschi, and Barry Trimmer. “Soft robotics: a bioinspired evolution in robotics”. In: *Trends in Biotechnology* 31.5 (2013), pp. 287–294. ISSN: 0167-7799. DOI: https://doi.org/10.1016/j.tibtech.2013.03.002. URL: https://www.sciencedirect.com/science/article/pii/S0167779913000632.

[5] Cecilia Laschi, Barbara Mazzolai, and Matteo Cianchetti. “Soft robotics: Technologies and systems pushing the boundaries of robot abilities”. In: *Science Robotics* 1.1 (2016), eaah3690. DOI: 10.1126/scirobotics.aah3690. eprint: https://www.science.org/doi/pdf/10.1126/scirobotics.aah3690. URL: https://www.science.org/doi/abs/10.1126/scirobotics.aah3690.

[6] Andrew D. Marchese, Robert K. Katzschmann, and Daniela Rus. “A recipe for Soft Fluidic Elastomer Robots”. In: *Soft Robotics* 2.1 (2015), pp. 7–25. DOI: 10.1089/soro.2014.0022.

[7] Tuan D. Ngo et al. “Additive manufacturing (3D printing): A review of materials, methods, applications and challenges”. In: *Composites Part B: Engineering* 143 (2018), pp. 172–196. ISSN: 1359-8368. DOI: https://doi.org/10.1016/j.compositesb.2018.02.012. URL: https://www.sciencedirect.com/science/article/pii/S1359836817342944.

[8] Ryuma Niiyama et al. “Pouch Motors: Printable Soft Actuators Integrated with Computational Design”. In: *Soft Robotics* 2 (May 2015), p. 150508072946000. DOI: 10.1089/soro.2014.0023.

[9] Daniela Rus and Michael T. Tolley. “Design, fabrication and control of soft robots”. In: *Nature* 521.7553 (May 2015), pp. 467–475. ISSN: 1476-4687. DOI: 10.1038/nature14543. URL: https://doi.org/10.1038/nature14543.

[10] Robert F. Shepherd et al. “Multigait soft robot”. In: *Proceedings of the National Academy of Sciences* 108.51 (2011), pp. 20400–20403. DOI: 10.1073/pnas.1116564108. eprint: https://www.pnas.org/doi/pdf/10.1073/pnas.1116564108. URL: https://www.pnas.org/doi/abs/10.1073/pnas.1116564108.

[11] J. Szulżyk-Cieplak, A. Duda, and B Sidor. “3D printers – new possibilities in education”. English. In: *Advances in Science and Technology Research Journal* Vol. 8, nr 24 (2014), pp. 96–101.

[12] L.E. Weiss et al. “Shape deposition manufacturing of heterogeneous structures”. In: *Journal of Manufacturing Systems* 16.4 (1997), pp. 239–248. ISSN: 0278-6125. DOI: https://doi.org/10.1016/S0278-6125(97)89095-4. URL: https://www.sciencedirect.com/science/article/pii/S0278612597890954.

[13] Shuhang Zhang. “A Monolithic fabrication of pouch actuated soft robots”. PhD thesis. UC San Diego, 2021, pp. 1–65.